

Received November 22, 2021, accepted November 30, 2021, date of publication December 8, 2021, date of current version December 20, 2021.

Digital Object Identifier 10.1109/ACCESS.2021.3133960

# Performance Optimization Analysis of Hybrid Excitation Generator With the Electromagnetic Rotor and Embedded Permanent Magnet Rotor for Vehicle

HUIHUI GENG<sup>1</sup>, XUEYI ZHANG<sup>1</sup>, LANIAN TONG<sup>2</sup>, QINGZHI MA<sup>2</sup>, MINGJUN XU<sup>1</sup>, YUFENG ZHANG<sup>1</sup>, AND LEI WANG<sup>3</sup>

<sup>1</sup>School of Transportation and Vehicle Engineering, Shandong University of Technology, Zibo 255049, China

<sup>2</sup>Research and Development Center, Shandong Tangjun Ouling Automobile Manufacture Company Ltd., Zibo 255049, China

<sup>3</sup>Technology Center, Weifang No. 1 Motor Factory Company Ltd., Weifang 262127, China

Corresponding author: Xueyi Zhang (zhangxueyi@sdut.edu.cn)

This work was supported in part by the National Natural Science Foundation of China under Grant 51875327 and Grant 51975340.

**ABSTRACT** To solve the problems of the non-adjustable magnetic field of the permanent magnet (PM) generator, large excitation loss and high failure rate of electric excitation generator, this paper proposes a parallel electromagnetic and PM hybrid excitation generator (HEG). The designed generator adopts a high power density PM rotor composed of built-in tangential PM steel and V-shaped PM steel and a salient-pole electromagnetic rotor (EMR) with short axial length, less electromagnetic loss, simple and reliable structure. By adjusting the axial length of two rotors and the size of magnetomotive force sources, the generator can adjust the rotor power distribution to meet various power requirements. Meanwhile, the HEG can adjust the electromagnetic magnetic field (EMMF) by adjusting the size and direction of the excitation current, and then can adjust the size of the synthetic magnetic field to achieve the purpose of stabilizing output voltage. In this paper, the magnetic circuit model of the HEG is established by using the equivalent magnetic circuit (EMC) method, and the rationality of the designed magnetic circuit is verified and analyzed by the finite element method. The prototype is trial-manufactured and tested, and the results show that the designed HEG has a wide magnetic regulation range, stable output voltage, and good output performance.

**INDEX TERMS** Combined-pole rotor, equivalent magnetic circuit method, hybrid excitation generator, vehicles.

## I. INTRODUCTION

Hybrid excitation generator (HEG) for vehicle not only has the characteristics of high efficiency and high power density of the permanent magnet (PM) generator but also has the flexible magnetic field regulation of the electric excitation generator [1]–[5]. Moreover, it can solve the problem that the magnetic field of the pure PM generator is not adjustable, and the output voltage increases linearly with the increase of the speed, which causes the output voltage to be difficult to stabilize. And it has become the development direction of vehicle generators in the future [6], [7]. For the hybrid

excitation power generation system, many researchers have carried out a lot of research. And the hybrid excitation topology mainly includes three types: PM steel in stator, PM steel in rotor, and parallel structure [8]–[10]. Most generator types of “PM steel in stator” are flux-switching machines. In this structure, the stator is usually composed of several toothed blocks to form a circular ring, the PM steel is embedded in the middle of the connection of two stator blocks, and the electromagnetic winding (EMW) is wound on the outside of the PM steel or on the adjacent stator teeth to form a hybrid excitation structure [11]–[14]. For example, reference [15] proposed a C-type hybrid excitation flux-switching machine. Its stator was spliced by C-type stator blocks, the PM steel was embedded in the splice, and the EMW was wound on the

The associate editor coordinating the review of this manuscript and approving it for publication was Jing Yan.

outside of the PM steel. Reference [16] proposed an E-type hybrid excitation flux-switching motor, which can reduce the PM steel by half compared with the C-type structure. The type of “PM steel in rotor” usually designs PM steel inside the rotor core and winds EMW around the rotor pole or the stator [17]–[19]. For example, reference [20] proposed a HEG with an adjustable magnetic field. Its EMW was axially wound on the left and right sides of the stator, and the PM steel was tangentially embedded in the rotor core. A salient pole hybrid excitation synchronous generator was proposed in [21]. Its rotor was composed of two salient poles and four PM poles. The EMW was wound on the salient pole, and the PM steel was embedded in the PM pole. The type of “parallel structure” is usually designed with its PM rotor and electromagnetic rotor (EMR) in parallel and coaxial, and the magnetic field generated by them is synthesized in the main air gap [22]–[24]. For example, reference [25] proposed a hybrid excitation motor with claw-pole rotor and surface-mounted PM rotor in parallel. In this structure, the EMW is axially wound inside of the inner end of the rotor, and the PM steel is attached to both sides of the claw pole to form the outer end of the rotor. Reference [26] proposed a hybrid excitation motor with a magnetic bypass structure. In this motor, the EMW is on the outside of the stator, and the electromagnetic magnetic field (EMMF) is transmitted to the stator through a special magnetic conductor.

To sum up, the EMMF of the type of “PM steel in stator” usually passes through the PM steel, which has some problems such as large magnetoresistance of the EMMF and irreversible demagnetization of the PM steel. Whereas, the circuit of EMMF in the type of “PM steel in rotor” is usually long and has many additional air gaps, which can lead to the low magnetic field regulation efficiency. The EMMF and PM magnetic field of the “parallel structure” are relatively independent and do not affect each other. The efficiency of magnetic field regulation is high, but the axial length of the rotor increases, and the volume of HEG is relatively large [27], [28]. Through comprehensive comparison, the “parallel structure” has the advantages of small excitation loss and good magnetic regulation characteristics, and it has excellent development potential. Therefore, the paper proposes a parallel structure HEG. The structure adopts a new type of combined-pole PM rotor with a pair of V-shaped PM steel in the middle of two built-in tangential PM steels. The rotor magnetic field of each pole of this design jointly provided by multiple PM steels, which has high magnetic field strength and high power density, and can effectively avoid the depression of the induced electromotive force’ peak caused by the weak magnetic field in the center of the rotor pole of single PM steel structure. The EMR adopts a salient-pole structure with simple structure and short axial length. Compared with the traditional claw-pole structure, the excess space of the axial EMW is much less than the length of the yoke of the claw pole. Therefore, the effective axial length of the synthetic rotor is reduced, which can effectively reduce the effective axial length of the stator core and armature

winding, and can effectively reduce copper consumption. The performance comparison between the designed HEG and the existing parallel HEG is shown in Table 1.

It can be seen from Table 1 that the PM part of parallel HEG mainly adopts the surface-mounted structure or built-in tangential PM rotor. For the surface-mounted PM rotor, the rotation of the rotor of high-speed generator is easy to cause the PM steel to fall off due to centrifugal force. Moreover, since the PM steel faces the main air gap directly, the armature reaction magnetic field passes through it directly, which is easy to cause the demagnetization of PM steel under high-power conditions. For the built-in tangential PM rotor, the PM steel is built on both sides of the rotor magnetic pole. Based on the principle of minimum magnetic circuit, the magnetic field generated by PM steel is mostly distributed on both sides of the PM steel, that is, on both sides of the rotor magnetic pole. It can lead to the weak magnetic field in the center of the rotor magnetic pole, uneven magnetic field distribution in the main air gap, and depression of the induced electromotive force’ peak [35]–[37]. In order to solve these problems, a combined-pole PM rotor is proposed in this paper. Compared with the conventional tangential PM rotor, two V-shaped PM steels are added in the middle of the two tangential PM steels. This design has a significant gathering effect of magnetic field and high rotor power density compared with the conventional rotor.

Table 1 also shows that the electromagnetic part of parallel HEG mainly adopts claw-pole structure, variable claw-pole structure, flux modulation generator, or inductor generator. Among them, the effective axial length of the conventional claw pole is in the middle of the claw, and there is an extended length of claw pole’ yoke on both sides. Therefore, in the middle of the two parallel rotors, the yoke of the claw pole occupies part of the axial length, which increases the volume and armature winding loss of the HEG. The variable claw-pole structure usually adopts a special magnetic conduction structure to introduce the PM magnetic field or the EMMF into the main air gap. The magnetic circuit of this kind of structure is usually long, and there are many additional air gaps. Moreover, the magnetic conduction structure distributed on both sides of the axial direction also increases the volume of the HEG. And the HEG using flux modulation generator and inductor generator instead of electromagnetic part mainly adopts double stator and double armature winding structure, which leads to the complexity of its structure and control system. Considering these problems, the salient-pole EMR is adopted in this paper. The rotor has a simple structure, flexible axial length adjustment, no additional air gap, and small magnetoresistance. Meanwhile, the axial length of the EMW is short, which does not occupy the volume of the HEG.

Compared with the parallel HEG currently developed, the designed HEG has significant advantages and better output performance. Meanwhile, the HEG can adjust the power distribution of two rotors by adjusting the axial length and magnetic potential source of the PM rotor and the EMR, so as

TABLE 1. Performance comparison of parallel HEG.

Name	PM rotor part	EMR part	Stator part	Advantages	Disadvantages
Claw-pole and built-in PM HEG <sup>[29]</sup>	Built-in tangential PM rotor	Claw-pole EMR	One stator core and one set of armature windings	The power adjustment range is extensive, and the power is easy to distribute.	The claw pole yoke located in the center of the two rotors occupies the effective length of the stator.
Claw-pole and surface mounted PM HEG <sup>[25]</sup>	The PM steel is pasted on the brackets on both sides of claw.	Variable claw-pole EMR with claw separated from yoke	One stator core and one set of armature windings	The space on both sides of the claw pole is effectively used, and the volume of the HEG is small.	The PM magnetic field is weak, the structure is complex, and the structural strength is low.
Hybrid excitation power generation with bypass magnetic circuit <sup>[26]</sup>	Built-in tangential PM rotor	Bypass EMR with variable claw-pole magnetic bridge	One stator core and one set of armature windings	The magnetic bridge is used to transfer the EMMF to reduce the effective axial length.	Two air gaps are added in the EMR, the magnetic circuit of EMMF is long, and the magnetic resistance increases.
Flux modulated HEG <sup>[30-33]</sup>	Surface-mounted PM rotor	Magnetic flux modulation electromagnetic part	Parallel double stator and parallel double armature windings	The power adjustment range is extensive, and the power is easy to distribute.	The combination of two types of power generation forms has a complex structure and complex control system.
PM-Inductor HEG <sup>[34]</sup>	Surface-mounted PM rotor	Inductor power generation part	One stator core and one set of armature windings	The power adjustment range is extensive, and the power is easy to distribute.	The axial length of the generator is greatly increased, and the efficiency of the inductive power generation part is low.
The HEG designed in this paper	Buil-in combined-pole PM rotor	Salient-pole EMR	One stator core and one set of armature windings	The structure is simple and reliable, the power adjustment range is extensive, and the power is easy to distribute.	The axial length is the sum of the axial lengths of two rotors.

to meet a variety of power requirements. From the above, the designed HEG has high research value.

The rest of this paper is organized as follows. Section II analyzes the magnetic field of the HEG, establishes the equivalent magnetic circuit (EMC) model, and carries out analytical calculation. Section III establishes the finite element analysis model of the HEG and solves its electromagnetic parameters to compare and analyze the effectiveness of the EMC method. Meanwhile, the magnetic field distribution and magnetic field regulation characteristics are analyzed to verify the rationality of the magnetic field design. Section IV uses the finite element method and prototype test method to analyze the output performance and application performance of the designed HEG. Finally, conclusions are drawn in Section V.

II. STRUCTURE AND MAGNETIC CIRCUIT MODEL OF HEG

The rotor of HEG is composed of salient-pole EMR and combined-pole PM rotor. Two rotors are coaxial and installed in parallel. The center of the two rotors is designed with magnetic isolation bushing, which can not only reduce axial leakage magnetic flux but also reserve space for EMW of EMR. The structure of HEG is shown in Fig. 1, and the main technical parameters of the generator are shown in Table 2.

As shown in Fig. 1, the PM rotor of HEG is a combined-pole structure and composed of the tangential PM steel and V-shaped PM steel. In order to reduce the leakage flux, a semicircular air gap is set at the outer end of the tangential PM steel, a triangular air gap is set at its inner end,

TABLE 2. Main technical parameter of HEG.

Technical indicators	Parameter value
Rated voltage $U_N$ (V)	28
Rated power $P_N$ (W)	1000
Rated speed $n_N$ (r/min)	4000
Number of phases $m$	3
Working mode	Continuous work
Working temperature	-40°C - 75°C
Insulation class	E
Output mode	Direct-current

a wedge-shaped air gap is set at the outer end of the V-shaped PM steel, and a through V-shaped air gap is set at the inside of two V-shaped PM steels.

For the designed combined-pole PM rotor, the magnetic field of the rotor is mainly based on the magnetic field provided by the tangential PM steel, and the magnetic field of the V-shaped PM steel plays an auxiliary role. The magnetic flux of each pole is jointly provided by multiple PM steels, and its magnetic circuit analysis diagram is shown in Fig. 2.

Under one magnetic pole of PM rotor, the main magnetic circuit of PM steel is: N pole of tangential PM steel → rotor core → air gap → stator core → air gap → rotor core → S pole of tangential PM steel → rotor core → N pole of tangential PM steel. As shown in the main magnetic circuit 1 in Fig. 2. Meanwhile, the V-shaped PM steel

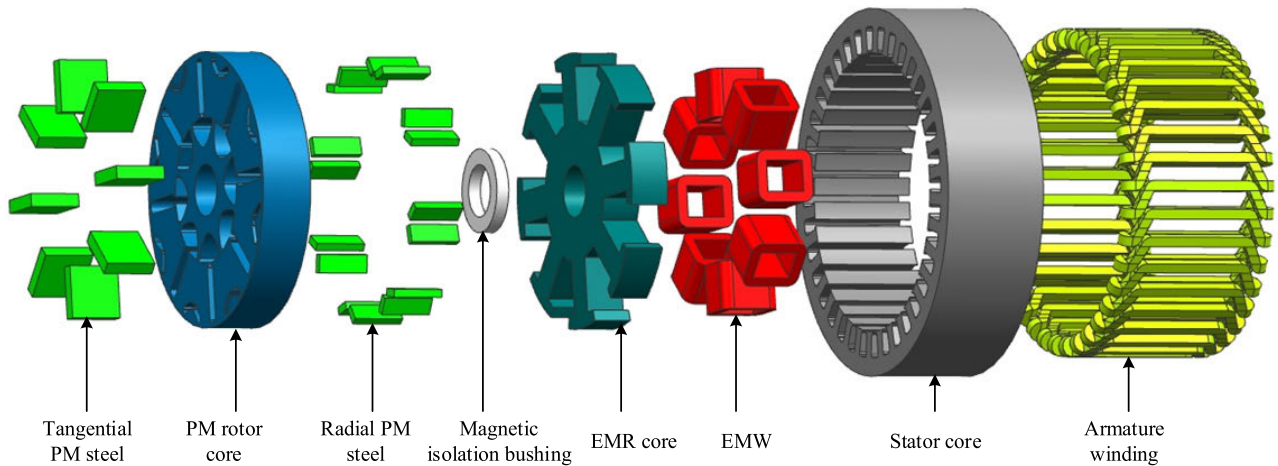


FIGURE 1. The structure of HEG.

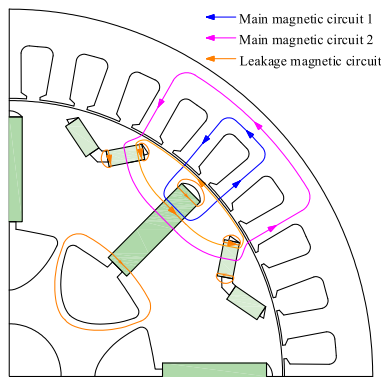


FIGURE 2. Magnetic circuit diagram of the PM rotor.

is built in the center of the rotor pole, and the polarity of it is opposite to that of tangential PM steel under one rotor pole. Therefore most of the magnetic field generated by tangential PM steel will go to the main air gap pass through V-shaped PM steel directly. This part of the magnetic circuit is: N pole of tangential PM steel → rotor core → S pole of V-shaped PM steel → air gap → stator core → air gap → N pole of V-shaped PM steel → rotor core → S pole of tangential PM steel → rotor core → N pole of tangential PM steel. It can be seen in the main magnetic circuit 2 in Fig. 3.

In order to simplify the analysis, the two main magnetic circuits are calculated separately, and the total magnetic flux of each pole is calculated as the sum of the magnetic flux of main magnetic circuit 1 and main magnetic circuit 2. Among them, the tangential PM steel provides the magnetic field in two main magnetic circuits, respectively. Therefore, its magnetomotive force and internal magnetic conductivity in each main magnetic circuit are calculated by half. Moreover, since the leakage magnetic circuit can be calculated only once, the leakage fluxes at the inner end and the outer end of the tangential PM steel are calculated in the main magnetic circuit 1, and the remaining leakage fluxes are calculated in

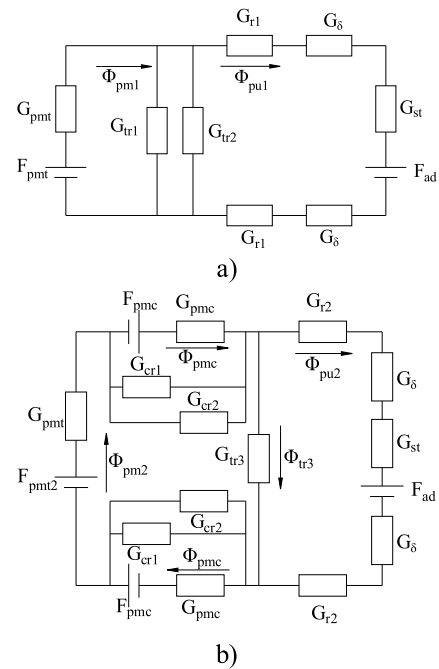


FIGURE 3. EMC diagram of PM rotor. a) The main magnetic circuit 1. b) The main magnetic circuit 2.

the main magnetic circuit 2. Based on this, the EMC diagrams of main magnetic circuit 1 and main magnetic circuit 2 of PM rotor are shown in Fig. 3.

In Fig. 3,  $F_{pmt}$  and  $F_{pmc}$  are the magnetomotive force of the tangential PM steel and the V-shaped PM steel, respectively,  $F_{ad}$  is the reaction magnetomotive force in direct axis, and under the no-load condition,  $F_{ad} = 0$ .  $\Phi_{pmt1}$  and  $\Phi_{pmt2}$  are the magnetic flux generated by the tangential PM steel in the magnetic circuit 1 and the magnetic circuit 2 respectively,  $\Phi_{pmc}$  is the magnetic flux generated by the V-shaped PM steel,  $\Phi_{pu1}$  and  $\Phi_{pu2}$  are the effective main magnetic flux of magnetic circuit 1 and magnetic circuit 2, respectively,  $\Phi_{tr3}$  is the leakage magnetic flux of the leakage magnetic circuit in

the rotor core outside the tangential PM steel and V-shaped PM steel.  $G_{pmt}$  and  $G_{pmc}$  are the internal permeance of the tangential PM steel and the V-shaped PM steel respectively,  $G_{tr1}$  and  $G_{tr2}$  are the leakage permeance of the magnetic circuit at the inner and outer ends of the tangential PM steel in the rotor core, respectively,  $G_{cr1}$  and  $G_{cr2}$  are the leakage permeance of the magnetic circuit at the inner end and outer end of the V-shaped PM steel, respectively,  $G_{r1}$  and  $G_{r2}$  are the permeance of the rotor core of the magnetic circuit 1 and magnetic circuit 2, respectively,  $G_{\delta}$  is the permeance of the main air gap, and  $G_{st}$  is the permeance of the stator core.

To simplify the analysis, the permeances of the leakage magnetic circuit at the inner end and outer end of the tangential PM steel are combined into one magnetic circuit through the parallel formula. The combined total leakage magnetic flux is recorded as  $\Phi_{tr}$ , and the combined permeance is recorded as  $G_{tr}$ , where  $G_{tr} = G_{tr1} + G_{tr2}$ . Similarly, the permeances of the leakage magnetic circuit at the inner end and outer end of V-shaped PM steel are also calculated together. The combined total leakage magnetic flux is recorded as  $\Phi_{cr}$ , and the combined permeance is recorded as  $G_{cr}$ , where  $G_{cr} = G_{cr1} + G_{cr2}$ . The simplified EMC models of main magnetic circuit 1 and main magnetic circuit 2 are shown in Fig. 4.

The analytical equations of the simplified equivalent models of main magnetic circuit 1 and main magnetic circuit 2 can be solved by the node method of the magnetic circuit, respectively:

$$\begin{cases} \Phi_{pm1} = \Phi_{tr} + \Phi_{pu1} \\ F_{pmt} = \Phi_{pm1} \frac{1}{G_{pmt}} + \Phi_{tr} \frac{1}{G_{tr}} \\ \Phi_{tr} \frac{1}{G_{tr}} = \Phi_{pu1} \left( \frac{2}{G_{r1}} + \frac{2}{G_{\delta}} + \frac{1}{G_{st}} \right) + F_{ad} \end{cases} \quad (1)$$

$$\begin{cases} \Phi_{pmc} = \Phi_{pm2} + \Phi_{cr} \\ \Phi_{pmc} + \Phi_{cr} = \Phi_{pu2} + \Phi_{tr3} \\ \Phi_{pmc} \frac{1}{G_{pmc}} = F_{pmc} + \Phi_{cr} \frac{1}{G_{cr}} \\ F_{pmt} + 2F_{pmc} = 2\Phi_{pmc} \frac{1}{G_{pmc}} + \Phi_{pm2} \frac{1}{G_{pmt}} + \Phi_{tr3} \frac{1}{G_{tr3}} \\ \Phi_{tr3} \frac{1}{G_{tr3}} = \Phi_{pu2} \left( \frac{2}{G_{r2}} + \frac{2}{G_{\delta}} + \frac{1}{G_{st}} \right) + F_{ad} \end{cases} \quad (2)$$

By solving the two equivalent models respectively, the analytical expressions of main magnetic flux and leakage magnetic flux of each part can be obtained as follows (3) and (4), as shown at the bottom of the next page.

For the magnetic field of the PM rotor, the effective magnetic flux  $\Phi_{pu}$  in the main air gap can be calculated as the sum of the magnetic flux of two main magnetic circuits in the main air gap, and  $\Phi_{pu} = \Phi_{pu1} + \Phi_{pu2}$ . The magnetomotive force of the tangential PM steel in two main magnetic circuits is calculated by half. Therefore, the total magnetic

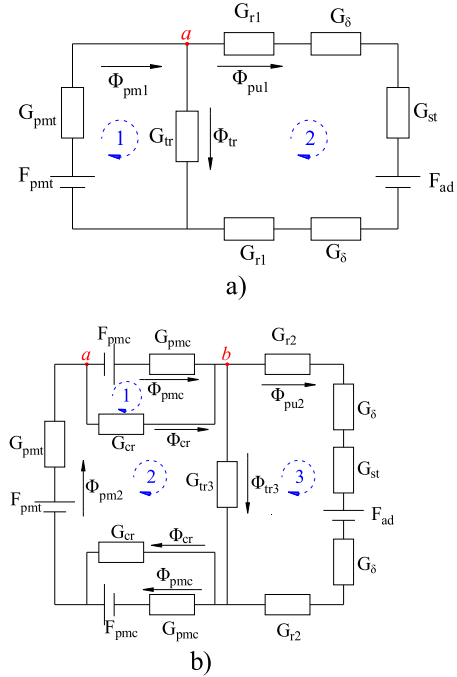


FIGURE 4. The simplified EMC model. a) The main flux magnetic circuit 1. b) The main flux magnetic circuit 2.

flux provided by the tangential PM steel  $\Phi_{pmt}$  is the sum of the magnetic flux provided by the tangential PM steel in the two main magnetic circuits, and  $\Phi_{pmt} = \Phi_{pm1} + \Phi_{pm2}$ . The magnetomotive force  $F_{pm}$  and the internal permeance  $G_{pm}$  of PM steel are calculated as follows:

$$\begin{cases} F_{pm} = \frac{B_r h_p}{\mu_p} \\ G_{pm} = \frac{\mu_0 \mu_p b_p L_p}{h_p} \end{cases} \quad (5)$$

where  $B_r$  is the remanence of PM steel,  $h_p$  is the length of PM steel in magnetization direction,  $\mu_p$  is the permeability of PM steel, and  $\mu_p = (1.05 \sim 1.1) \mu_0$ , where  $\mu_0$  is the permeability of vacuum,  $b_p$  is the width of PM steel, and  $L_p$  is the axial length of PM steel.

In equations (1) and (2), the magnetomotive force and internal permeance of tangential PM steel and V-shaped PM steel can be calculated according to the above formula, and the other permeance and leakage permeance can be calculated as:

$$\begin{cases} G_r = \frac{\mu_r A_r}{l_r} \\ G_{\delta} = \frac{\mu_0 \pi D_{il} L_{st}}{2P\delta} \\ G_{st} = \frac{\mu_r b_t L_{st}}{h_s} + \frac{Z \mu_r h_j L_{st}}{\pi (D_{il} + h_j) k_{st}} \end{cases} \quad (6)$$

where  $G_r$  is the permeance of magnetic circuit in rotor core,  $\mu_r$  is the permeability of rotor core,  $A_r$  is the cross-sectional area of rotor magnetic circuit, and  $A_r = L_r h_r$ , where,  $L_r$  is the axial length of the rotor core,  $h_r$  is the effective calculated



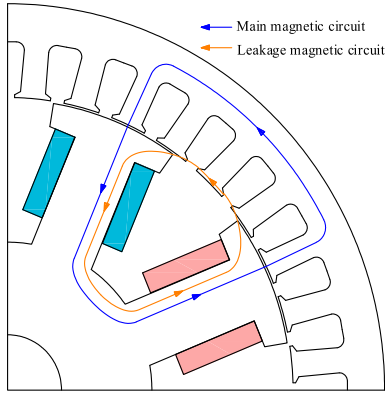


FIGURE 5. Magnetic circuit analysis diagram of EMR.

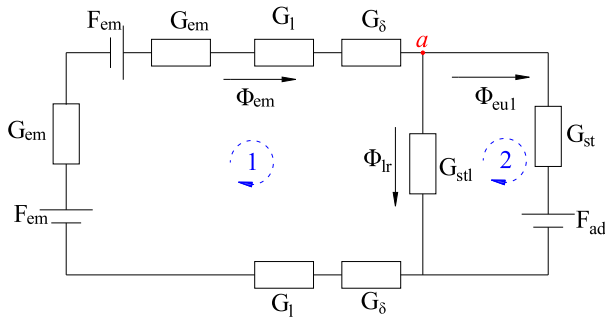


FIGURE 6. EMC diagram of EMMF.

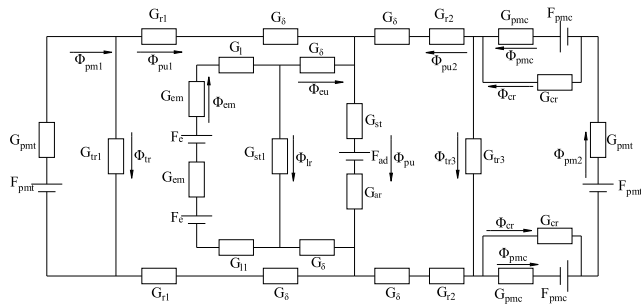


FIGURE 7. EMC diagram of the synthetic magnetic field.

In Fig. 6,  $F_{em}$  is the magnetomotive force generated by the EMW,  $\Phi_{em}$  is the total magnetic flux of the EMW,  $\Phi_{lr}$  is the leakage flux,  $\Phi_{eu}$  is the effective magnetic flux,  $G_{em}$  is the internal permeance of the EMW,  $G_l$  is the permeance of the main magnetic circuit in the EMR, and it can be calculated according to the calculation method of  $G_r$ , and  $G_{stl}$  is the permeance of the leakage magnetic circuit of the stator teeth. The EMC model of the EMMF can be established as follows:

$$\begin{cases} \Phi_{em} = \Phi_{lr} + \Phi_{eu} \\ 2F_{em} = \Phi_{em} \left( \frac{2}{G_{em}} + \frac{2}{G_l} + \frac{2}{G_\delta} \right) + \Phi_{lr} \frac{1}{G_{stl}} \\ \Phi_{lr} \frac{1}{G_{stl}} = \Phi_{eu} \frac{1}{G_{st}} + F_{ad} \end{cases} \quad (7)$$

The analytical expressions of magnetic flux obtained by solving the EMC model of the EMMF are as follows (8), as shown at the bottom of the next page.

Since the internal resistance of the EMW is very small,  $1/G_{em}$  is equivalent to 0, so it is ignored. The magnetomotive force generated by the EMW can be calculated as:

$$F_{em} = I_f N_f \quad (9)$$

where  $I_f$  is the current of the EMW, and  $N_f$  is the number of turns of the EMW.

The leakage permeance  $G_{stl}$  between the stator teeth is calculated as the leakage permeance with one tooth width and two slot widths, which can be calculated as:

$$G_{stl} = \frac{\mu_r L_{st} h_{s0} Z}{\pi D_{il} - Z b_{s0}} + \frac{2\mu_r L_{st} h_{s0}}{b_{s0}} \quad (10)$$

where  $h_{s0}$  is the height of stator slot wedge, and  $b_{s0}$  is the width of stator slot.

The synthetic magnetic field of the HEG is the synthesis of the PM magnetic field and the EMMF in the main air gap, and its EMC diagram is shown in Fig. 7.

In Fig. 7,  $G_{ar}$  is the leakage permeance between the PM rotor and the EMR. According to the EMC diagram, the total main magnetic flux of the HEG can be calculated as follows:

$$\Phi_u = \Phi_{pu} + \Phi_{eu} \quad (11)$$

The total coefficient of leakage magnetic flux of the HEG can be calculated as:

$$\sigma = \frac{\Phi_{pmt} + \Phi_{pmc} + \Phi_{em}}{\Phi_u} \quad (12)$$

### III. MAGNETIC FIELD SIMULATION ANALYSIS OF THE HEG

In order to analyze the output performance of the HEG, it's finite element model is established by using the finite element software, and is shown in Fig. 8.

To solve the magnetic flux, the solving surfaces of the magnetic flux  $a-i$  are drawn and shown in Fig. 9.

In Fig. 9, surface  $a$ , surface  $b$ , and surface  $c$  are used to solve the total magnetic flux generated by the tangential PM steel, the V-shaped PM steel, and the EMW respectively, surface  $d$  is used to solve the effective magnetic flux of per pole of the stator, surface  $e$  and surface  $f$  are used to solve the leakage magnetic flux at the outer end and the inner end of the tangential PM steel respectively, surface  $g$  and surface  $h$  are used to solve the leakage magnetic flux at the outer end and the inner end of the V-shaped PM steel respectively, and surface  $i$  is used to solve the leakage magnetic flux between two salient poles. Using the solving surfaces and the finite element model, we can calculate the magnetic flux of each part, and the result, compared with the EMC method, is shown in Table 3

As shown in Table 3, the magnetic flux of each part calculated by the EMC model is basically the same as that calculated by the finite element method, and the calculated leakage

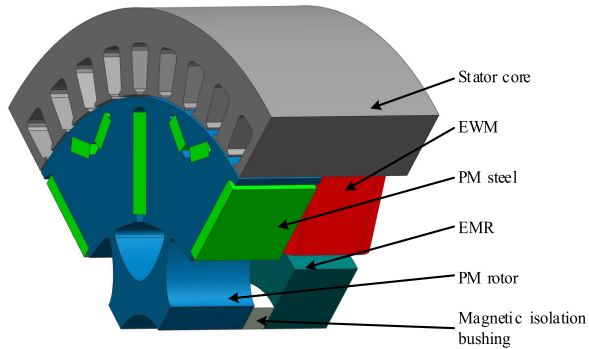


FIGURE 8. Finite element analysis model of HEG.

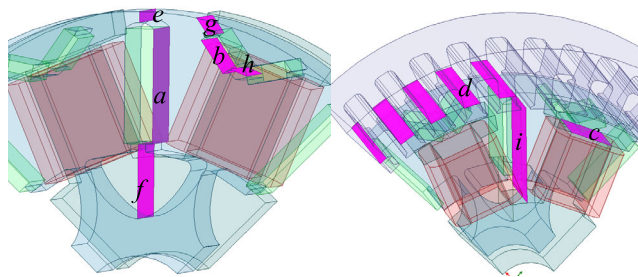


FIGURE 9. The solving surfaces of magnetic flux of HEG.

TABLE 3. Calculation table of the magnetic field parameters of HEG.

Calculation parameters	EMC method	Finite element method
Total magnetic flux generated by the tangential PM steel	$4.09 \times 10^{-4} \text{Wb}$	$4.34 \times 10^{-4} \text{Wb}$
Total magnetic flux generated by the V-shaped PM steel	$1.61 \times 10^{-4} \text{Wb}$	$1.45 \times 10^{-4} \text{Wb}$
Total magnetic flux generated by the EMW	$2 \times 10^{-4} \text{Wb}$	$2.32 \times 10^{-4} \text{Wb}$
Leakage flux at the out end and the inner end of the tangential PM steel	$1.12 \times 10^{-4} \text{Wb}$	$9.64 \times 10^{-5} \text{Wb}$
Leakage flux at the out end and the inner end of the V-shaped PM steel	$1.25 \times 10^{-5} \text{Wb}$	$1.36 \times 10^{-5} \text{Wb}$
Leakage flux between two salient poles	$1.59 \times 10^{-5} \text{Wb}$	$1.45 \times 10^{-5} \text{Wb}$
Effective magnetic flux in the stator teeth	$6.3 \times 10^{-4} \text{Wb}$	$6.23 \times 10^{-4} \text{Wb}$
Leakage magnetic flux coefficient	1.222	1.302

flux coefficient is 1.222, which is smaller than the result of the finite element method, but the result can prove that the

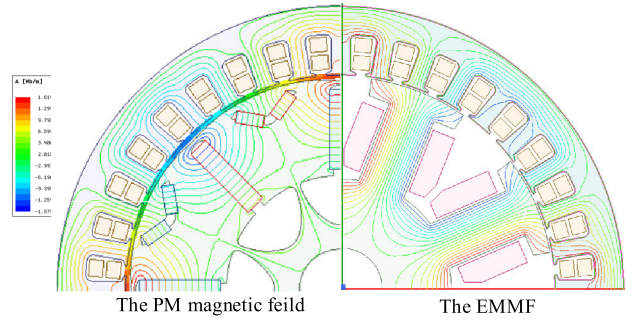


FIGURE 10. Distribution of the magnetic field lines of the HEG.

EMC method is reasonable. Using the finite element model, the distribution of the magnetic field of the PM magnetic field and the EMMF are simulated and shown in Fig. 10.

According to Fig. 10, the PM magnetic field is mainly based on the magnetic circuit 2. The leakage magnetic flux is mainly distributed at the ends of the tangential PM steel. Fig. 10 also shows that the distribution of magnetic field lines is the same as the analysis results of EMC, which can prove that the EMC design method is effective and is suitable for the design and analysis of hybrid excitation magnetic circuits.

The synthetic magnetic field of the HEG is mainly based on the PM magnetic field, which gives full play to the advantages of high magnetic field intensity and high power density of the PM rotor. Meanwhile, it will weaken the EMMF, reduce the excitation loss effectively and improve the output efficiency of the generator. The EMMF mainly plays a role in adjusting the size of the synthetic magnetic field and stabilizing the output voltage. The magnetic flux density vector diagram of the HEG under different excitation currents is simulated and shown in Fig. 11.

Fig. 11 shows that when the excitation current is positive, the direction of the EMMF is consistent with that of the PM magnetic field. Under this conduction, the EMMF plays the role of increasing the magnetic field, the synthetic magnetic field increases, and the output voltage of the generator increases too. When the excitation current is reversed, the direction of the EMMF is opposite to that of the PM magnetic field. Under this conduction, the EMMF plays the role of weakening the magnetic field, the synthetic magnetic field decreases, and the output voltage decreases too. It can also be seen in Fig. 11 that when the excitation current increases from 2A to 3A, the magnetic field intensity of the stator part corresponding to the EMR increases significantly, which

$$\begin{cases}
 \Phi_{em} = \frac{2F_{em}G_{\delta}G_{em}G_lG_{st} - F_{ad}G_{\delta}G_{em}G_lG_{st} + 2F_{em}G_{\delta}G_{em}G_lG_{stl}}{G_{\delta}G_{em}G_l + 2G_{\delta}G_{em}G_{st} + 2G_{\delta}G_{em}G_{stl} + 2G_{\delta}G_lG_{st} + 2G_{\delta}G_lG_{stl} + 2G_{em}G_lG_{st} + G_{em}G_lG_{stl}} \\
 \Phi_{eu} = \frac{2F_{em}G_{\delta}G_{em}G_lG_{st} - F_{ad}G_{\delta}G_{em}G_lG_{st} - 2F_{ad}G_{\delta}G_{em}G_{st}G_{stl} - 2F_{ad}G_{\delta}G_lG_{st}G_{stl} - 2F_{ad}G_{em}G_lG_{st}G_{stl}}{G_{\delta}G_{em}G_l + 2G_{\delta}G_{em}G_{st} + 2G_{\delta}G_{em}G_{stl} + 2G_{\delta}G_lG_{st} + 2G_{\delta}G_lG_{stl} + 2G_{em}G_lG_{st} + G_{em}G_lG_{stl}} \\
 \Phi_{lr} = \frac{2G_{stl}(F_{em}G_{\delta}G_{em}G_l + F_{ad}G_{\delta}G_{em}G_{st} + F_{ad}G_{\delta}G_lG_{st} + F_{ad}G_{em}G_lG_{stl})}{G_{\delta}G_{em}G_l + 2G_{\delta}G_{em}G_{st} + 2G_{\delta}G_{em}G_{stl} + 2G_{\delta}G_lG_{st} + 2G_{\delta}G_lG_{stl} + 2G_{em}G_lG_{st} + G_{em}G_lG_{stl}}
 \end{cases} \quad (8)$$

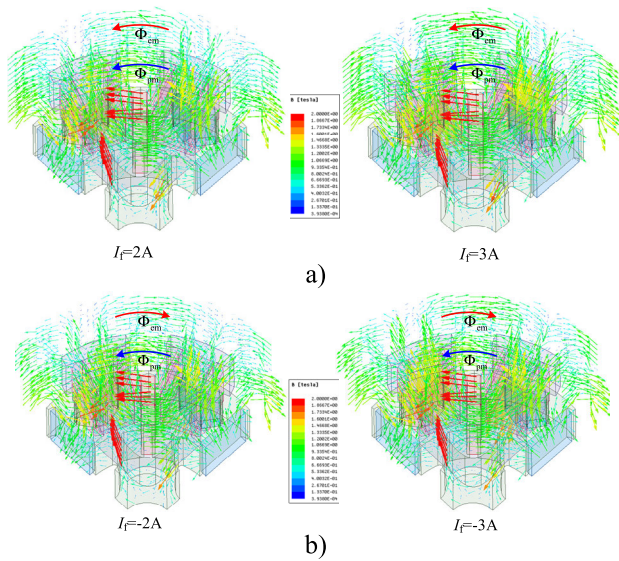


FIGURE 11. Magnetic flux density vector diagram of the HEG under different excitation currents. a) When  $I_f$  is forward. b) When  $I_f$  is reverse.

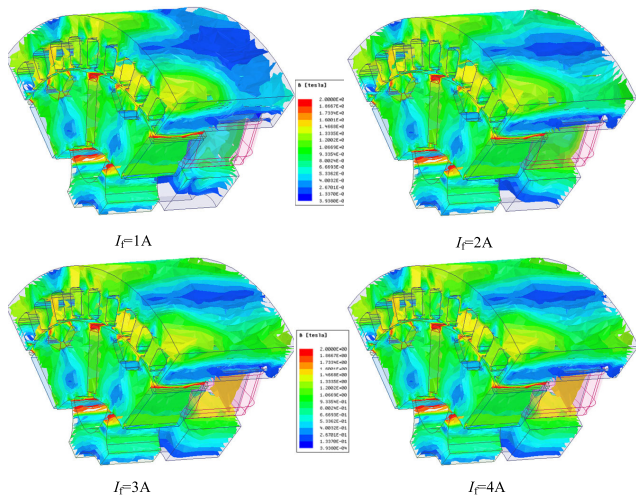


FIGURE 12. The magnetic flux density of HEG under different excitation currents.

shows that with the increase of the excitation current, the EMMF increases, and the increasing and weakening effect of the EMMF on the synthetic magnetic field increases. The diagram of the magnetic flux density of HEG under different excitation currents is shown in Fig. 12.

It can be seen from Fig. 12 that with the increase of excitation current, the magnetic flux density of the stator part corresponding to the EMR increases, the magnetic flux density of the stator teeth and stator yoke can reach 1.6T, and the distribution of magnetic field become more uniform. And when the excitation current increases to 4A, the main magnetic circuit of the PM rotor, the EMR, and the stator core does not reach saturation, which indicates that the EMR can still work normally when the excitation current is large, it can complete the role of increasing and reducing magnetic

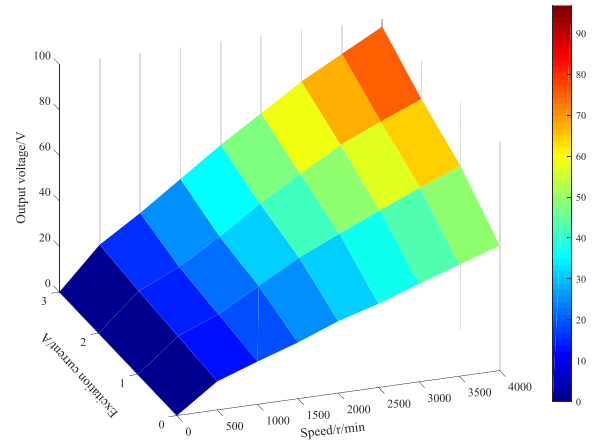


FIGURE 13. The output voltage of the HEG under different excitation currents and different speeds.

field. Fig. 12 also shows that the saturation of the magnetic field mainly exists at both ends of the tangential PM steel and the outer end of the V-shaped PM steel, these two parts are the leakage magnetic circuit, and those parts can force the magnetic flux to the effective magnetic flux path, increase the magnetic field strength of the main magnetic circuit and reduce the leakage flux loss. From the above analysis, the magnetic field design of HEG is reasonable.

IV. OUTPUT PERFORMANCE ANALYSIS OF HEG

When the excitation current increases from 0A to 3A, and the interval is 1A, the speed of the generator increases from 500r/min to 4000r/min, and the step is 500r/min, the output voltage of the HEG is simulated and shown in Fig. 13.

Fig. 13 shows that under the same speed, the output voltage of the HEG increases with the increase of the excitation current. And under the same excitation current, the output voltage increases almost linearly with the rise of the speed, which shows that the HEG has good regulation characteristics at different speeds. Set the generator speed is 3000r/min and the excitation current is 0A and 2A, respectively, the curve of output voltage with load current, namely external characteristic curve of the HEG, is simulated and shown in Fig. 14.

Fig. 14 shows that when the generator operates with the load, the speed and excitation current remain unchanged, the output voltage of the generator decreases linearly with the increase of load current. Therefore, to maintain the stable output voltage, it is necessary to adjust the size and direction of the excitation current continuously. It can also be seen that under the rated load, when the excitation current is 0A and 2A, the output voltage is 10V and 29V, respectively. It shows that when the speed is 3000r/min, the excitation current of 2A can ensure that the generator output voltage reaches the rated voltage. The calculated power characteristic curves under different excitation currents are shown in Fig. 15.

Fig. 15 shows that when the speed is 3000r/min, and the excitation current is 0A, the peak output power is 420W,

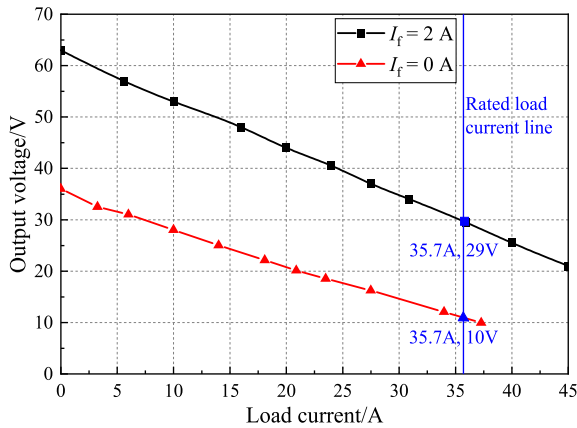


FIGURE 14. The external characteristic curve of the HEG.

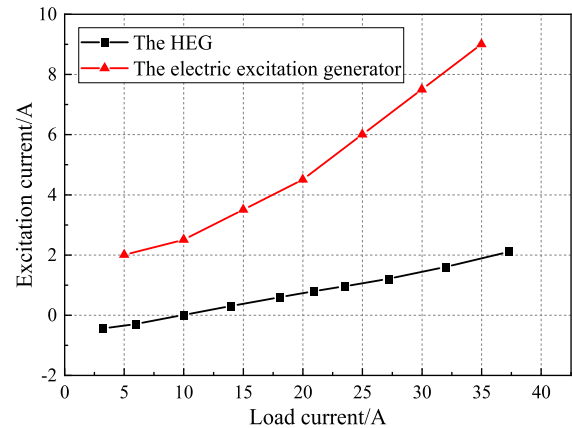


FIGURE 16. The regulation characteristic curves of HEG and electric excitation generator.

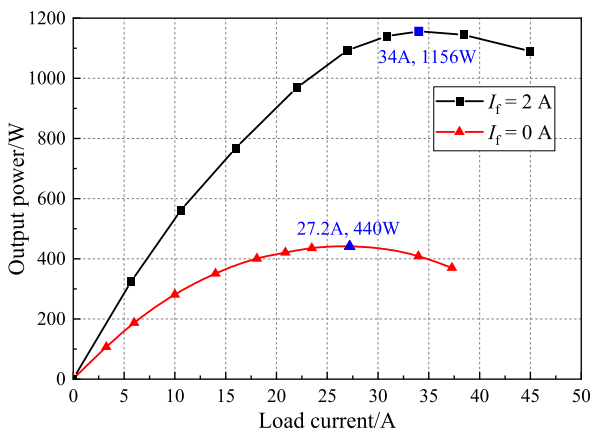


FIGURE 15. The power characteristic of the generator under different excitation currents.

whereas when the excitation current of the HEG is 2A, the peak output power is 1156W. And under the rated load condition, the output power is 1100W, which means that the HEG can ensure the rated power output under the rated condition.

When the speed of HEG is 3000 r/min, change the generator load, and stabilize the output voltage at the rated voltage by adjusting the excitation current, the relationship of the excitation current and the load current, namely the regulation characteristics, can be obtained. And the regulation characteristic curves of HEG and electric excitation generator are simulated and compared as shown in Fig. 16.

It can be seen from Fig. 16 that when the load current is small, the HEG needs to input reverse excitation current to weaken the air-gap magnetic field and maintain the output voltage at 28 V. With the increase of load current, to maintain the stability of output voltage, both HEG and electric excitation generator need to increase the excitation current, but the excitation current required by HEG is much less than that of electric excitation generator. Therefore, the HEG with low excitation current demand can avoid the problems of large excitation heating, large excitation loss, and the decline of output efficiency.

TABLE 4. Main structure parameters of HEG.

Parameter name	Parameter value	Parameter name	Parameter value
Outer diameter of the stator core ( mm )	140	Outer diameter of the rotor core ( mm )	105
Inner diameter of the stator core ( mm )	106	Inner diameter of the rotor core ( mm )	20
Axial length of the HEG ( mm )	45	Number of the rotor poles	8
The number of stator slots	36	Tangential PM steel ( mm )	20*20*5
Material of the PM steel	N38SH	V-shaped PM steel ( mm )	20*7*3
The turns of per slot of the armature winding	16	Wire diameter of the armature winding ( mm )	0.78
Silicon steel sheet material	DW310-35	The turns of per pole of the EMW	100
Length of the air gap ( mm )	0.5	Wire diameter of the EMW ( mm )	0.56

To verify the effectiveness of the simulation analysis, the prototype of the designed HEG is trial-manufactured, the test platform is built, and the prototype test is carried out. The main structural parameters of the HEG are shown in Table 4, and the prototype and test bench are shown in Fig. 17 and Fig. 18, respectively.

Under the rated speed condition of the generator, the no-load output voltage of the prototype when the excitation current in different directions and sizes is tested, and the no-load characteristic curve of the generator is obtained and shown in Fig. 19 with the simulation results.

It can be seen from Fig. 19 that the change trend of the no-load characteristic curve of the HEG obtained by prototype test and finite element analysis is consistent, and the values of test result are slightly smaller than the simulation result when the excitation current is large, but the maximum deviation between them is less than 5V, which proves that the simulation result of the HEG is effective. It can be seen

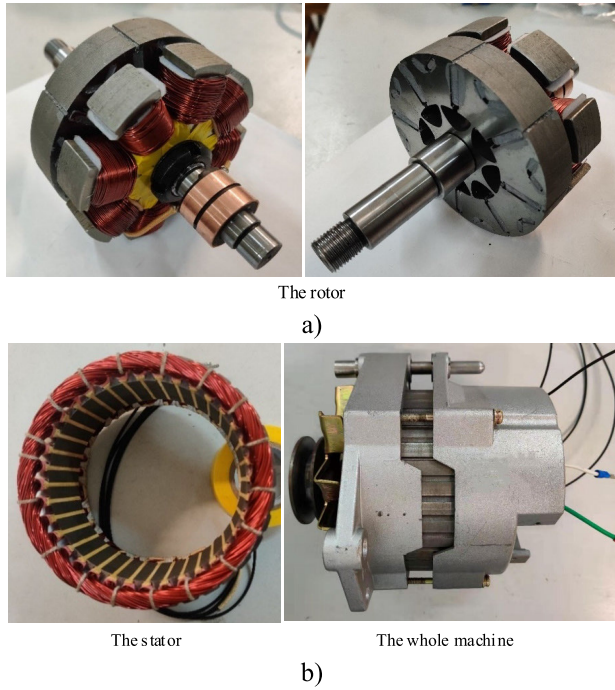


FIGURE 17. Each part of the prototype of HEG. a) The rotor. b) The stator and whole machine.

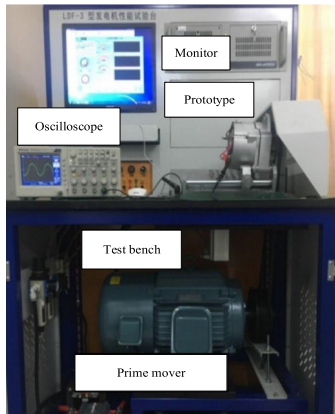


FIGURE 18. Generator test bench.

that when the excitation current changes from  $-3\text{A}$  to  $3\text{A}$ , the output voltage of the generator increases almost linearly with the increase of excitation current, from  $17\text{V}$  to  $92\text{V}$ , whereas when the excitation current, with forward or reverse direction, is greater than  $3\text{A}$ , the increasing and decreasing trend of the output voltage of the HEG decreases, at those time, the EMMF tends to be saturated and the regulation effect is weakened. Meanwhile, it shows that the HEG has a wide voltage regulation range, and the output voltage can change between  $11\text{V}$  to  $95\text{V}$  by changing the magnitude and direction of the excitation current.

When the speed of HEG is  $3000\text{ r/min}$ , and the excitation current is  $2\text{A}$ , the external characteristic of the HEG is tested and is shown in Fig.20 with the simulation result.

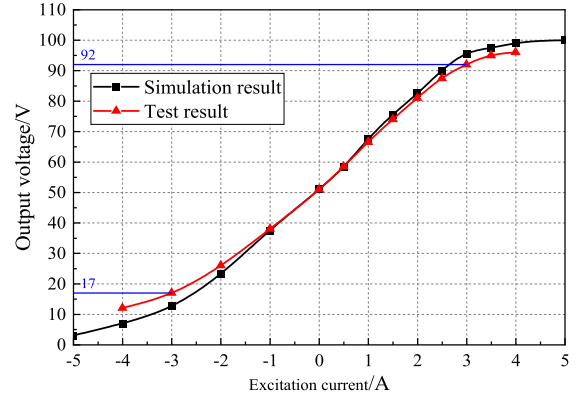


FIGURE 19. No-load characteristic of the HEG of test result and simulation result.

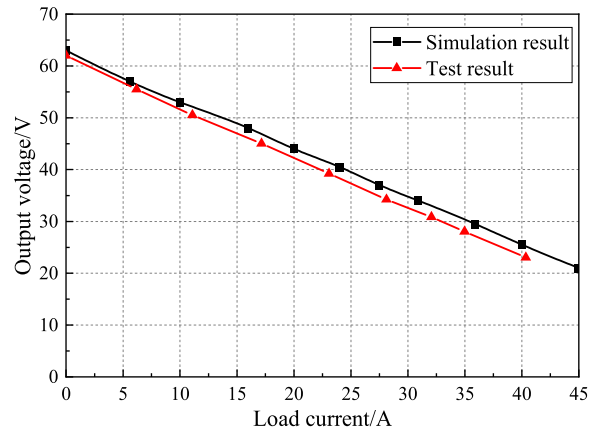


FIGURE 20. The external characteristic of the HEG of test result and simulation result.

It can be seen from Fig. 20 that the variation trend of the external characteristic curve of the HEG obtained by the prototype test and the simulation is consistent, and the deviation between them is more minor, which can verify the effectiveness of finite element analysis. Meanwhile, under the condition of constant generator speed and excitation current, the output voltage of the generator decreases almost linearly with the increase of load current, and the load current under rated load condition is  $35.7\text{A}$ , and the output voltage can reach  $28\text{V}$ . So, the generator can output rated voltage under rated working conditions.

When the speed of HEG is  $3000\text{ r/min}$ , changing the load of the generator, and stabilizing the output voltage at the rated voltage by adjusting excitation current, the regulation characteristic curves can be obtained by the test and the simulation, as shown in Fig. 21.

Fig. 21 shows that when the generator load is  $200\text{W}$ , the excitation current needs to be  $-0.6\text{A}$ . At this time, the direction of the EMMF is opposite to that of the PM magnetic field, the EMMF weakens the synthetic magnetic field to stabilize the output voltage at  $28\text{V}$ . When the generator is under the rated load condition, the excitation current is  $2.3\text{A}$ , the direction of the EMMF is the same as that of the PM magnetic field, the EMMF plays the role of increasing the

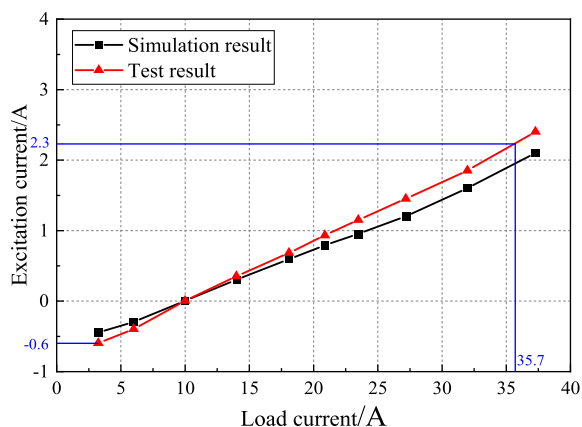


FIGURE 21. The magnetic regulation characteristic curve of HEG.

TABLE 5. Output voltage test results of the HEG.

Speed(r/min)	Load power(W)	Output voltage(V)
2000	980	27.6
	1000	27.1
	1200	26.3
4000	980	28.3
	1000	28.4
	1200	28.2
4800	980	28.6
	1000	28.6
	1200	28.5

synthetic magnetic field, and ensuring that the output voltage rises to 28V. Therefore, the stability of output voltage can be effectively guaranteed by changing the excitation current.

When the load power of the HEG is 980W, 1000W, and 1020W, respectively, the performance test of the HEG is carried out from low speed to high speed, and the results are shown in Table 5.

It can be seen from Table 5 that when the generator speed changes from 2000 r/min to 4800 r/min and the load power changes from 980W to 1020W, the HEG can stabilize the output voltage between 26.3V and 28.6V, it means that the design of HEG is effective.

V. CONCLUSION

The paper proposes a HEG with salient-pole EMR and combined-pole PM rotor in parallel and coaxial. The generator is mainly composed of PM magnetic field and assisted by EMMF, so as to have the advantages of high power density, less electromagnetic loss, large magnetic field strength, and wide magnetic regulation range. The magnetic circuit models of the PM magnetic field, the EMMF, and the synthetic magnetic field are established by using the EMC method. And used this model, the magnetic flux of PM steel and the EMW, the leakage magnetic flux and the effective magnetic flux are

calculated to get the leakage flux coefficient, and the result is 1.222. To verify the effectiveness of the EMC method, the finite element model is established and analyzed by finite element software. Meanwhile, the magnetic field regulation characteristic of the HEG is analyzed by the finite element model. It shows that changing the size and direction of excitation current can effectively change the size and direction of the EMMF and the size of the synthetic magnetic field, so as to achieve the purpose of stabilizing output voltage. The prototype is trial-manufactured and tested. And the results show that when the excitation current is from -3A to 3A, the output voltage of the designed HEG increases almost linearly from 15V to 90V, under the rated load condition, the output voltage can be stable at 28V, and the designed HEG has good voltage stabilizing performance.

REFERENCES

- [1] Q. Lu, B. Wu, Z. Zeng, and X. Huang, "Analysis of a new partitioned-primary flux-reversal hybrid-excited linear motor," *IEEE Trans. Ind. Appl.*, vol. 57, no. 1, pp. 448-457, Jan. 2021, doi: 10.1109/TIA.2020.3040205.
- [2] E. F. Farahani, M. A. J. Kondelaji, and M. Mirsalim, "An innovative hybrid-excited multi-tooth switched reluctance motor for torque enhancement," *IEEE Trans. Ind. Electron.*, vol. 68, no. 2, pp. 982-992, Feb. 2021, doi: 10.1109/TIE.2020.2969073.
- [3] L. Wei, T. Nakamura, and K. Imai, "Development and optimization of low-speed and high-efficiency permanent magnet generator for micro hydro-electrical generation system," *Renew. Energy*, vol. 147, pp. 1653-1662, Mar. 2020. [Online]. Available: <https://www.sciencedirect.com/science/article/pii/S0960148119313795>, doi: 10.1016/j.renene.2019.09.049.
- [4] X. Zhang, Q. Du, S. Ma, H. Geng, W. Hu, Z. Li, and G. Liu, "Permeance analysis and calculation of the double-radial rare-earth permanent magnet voltage-stabilizing generation device," *IEEE Access*, vol. 6, pp. 23939-23947, 2018, doi: 10.1109/ACCESS.2018.2792448.
- [5] H. Geng, X. Zhang, Y. Zhang, W. Hu, Y. Lei, X. Xu, A. Wang, S. Wang, and L. Shi, "Development of brushless claw pole electrical excitation and combined permanent magnet hybrid excitation generator for vehicles," *Energies*, vol. 13, no. 18, pp. 1-13, Sep. 2020, doi: 10.3390/en13184723.
- [6] A. S. Al-Adsani and O. Beik, "Characterization of a hybrid PM generator using a 32-phase brushless excitation scheme," *IEEE Trans. Energy Convers.*, vol. 34, no. 3, pp. 1391-1400, Sep. 2019, doi: 10.1109/TEC.2019.2910502.
- [7] W. Hu, X. Zhang, H. Geng, T. Gao, L. Shi, and D. You, "Electromagnetic design and flux regulation analysis of new hybrid excitation generator for electric vehicle range extender," *J. Electr. Comput. Eng.*, vol. 2021, pp. 1-13, Mar. 2021, doi: 10.1155/2021/5547517.
- [8] Z. Q. Zhu, N. Pothi, P. L. Xu, and Y. Ren, "Uncontrolled generator fault protection of novel hybrid-excited doubly salient synchronous machines with field excitation current control," *IEEE Trans. Ind. Appl.*, vol. 55, no. 4, pp. 3598-3606, Jul./Aug. 2019, doi: 10.1109/TIA.2019.2909492.
- [9] W. Ding, S. Yang, and Y. Hu, "Performance improvement for segmented-stator hybrid-excitation SRM drives using an improved asymmetric half-bridge converter," *IEEE Trans. Ind. Electron.*, vol. 66, no. 2, pp. 898-909, Feb. 2019, doi: 10.1109/TIE.2018.2833034.
- [10] W. Hu, X. Zhang, H. Yin, H. Geng, Y. Zhang, and L. Shi, "Analysis of magnetic field and electromagnetic performance of a new hybrid excitation synchronous motor with dual-V type magnets," *Energies*, vol. 13, no. 6, p. 1501, Mar. 2020, doi: 10.3390/en13061501.
- [11] Y. Du, J. Zhao, F. Xiao, X. Zhu, L. Quan, and F. Li, "Partitioned stator hybrid excitation doubly salient machine with slot Halbach PM arrays," *IEEE Trans. Veh. Technol.*, vol. 70, no. 4, pp. 3187-3196, Apr. 2021, doi: 10.1109/TVT.2021.3065670.
- [12] T. Okada, H. Matsumori, T. Kosaka, and N. Matsui, "Hybrid excitation flux switching motor with permanent magnet placed at middle of field coil slots and high filling factor windings," *CES Trans. Electr. Mach. Syst.*, vol. 3, no. 3, pp. 248-258, Sep. 2019. [Online]. Available: <https://ieeexplore.ieee.org/document/8858073>, doi: 10.30941/CESTEMS.2019.00033.

- [13] H. Ali, E. Sulaiman, R. Aziz, M. Jenal, M. Z. Ahmad, and F. Khan, "Review of double stator flux switching machines with various arrangements of excitation sources," *Alexandria Eng. J.*, vol. 60, no. 5, pp. 4393–4410, Oct. 2021, doi: [10.1016/j.aej.2021.03.022](https://doi.org/10.1016/j.aej.2021.03.022).
- [14] N. Ahmad, F. Khan, H. Ali, S. Ishaq, and E. Sulaiman, "Outer rotor wound field flux switching machine for in-wheel direct drive application," *IET Electr. Power Appl.*, vol. 13, no. 6, pp. 757–765, 2019, doi: [10.1109/TPVT.2021.3065670](https://doi.org/10.1109/TPVT.2021.3065670).
- [15] W. Hua, M. Cheng, and G. Zhang, "A novel hybrid excitation flux-switching motor for hybrid vehicles," *IEEE Trans. Magn.*, vol. 45, no. 10, pp. 4728–4731, Oct. 2009, doi: [10.1109/TMAG.2009.2022497](https://doi.org/10.1109/TMAG.2009.2022497).
- [16] J. T. Chen, Z. Q. Zhu, S. Iwasaki, and R. Deodhar, "A novel E-core flux-switching PM brushless AC machine," in *Proc. IEEE Energy Convers. Congr. Expo.*, Sep. 2010, pp. 3811–3818, doi: [10.1109/ECCE.2010.5618332](https://doi.org/10.1109/ECCE.2010.5618332).
- [17] M. Z. Ahmad, E. Sulaiman, Z. A. Haron, and T. Kosaka, "Impact of rotor pole number on the characteristics of outer-rotor hybrid excitation flux switching motor for in-wheel drive EV," *Proc. Technol.*, vol. 11, pp. 593–601, Jan. 2013, doi: [10.1016/j.protec.2013.12.233](https://doi.org/10.1016/j.protec.2013.12.233).
- [18] S. Yao and W. Zhang, "Stator tooth shape optimization for double salient hybrid excitation generator based on asymmetric circuit analysis," *COMPEL Int. J. Comput. Math. Electr. Electron. Eng.*, vol. 38, no. 6, pp. 1738–1755, Oct. 2019. [Online]. Available: <https://www.emerald.com/insight/content/doi/10.1108/COMPEL-09-2018-0344/full/html>, doi: [10.1108/COMPEL-09-2018-0344](https://doi.org/10.1108/COMPEL-09-2018-0344).
- [19] Z. Shushu, L. Chuang, N. Yinhang, and T. Jie, "A two-stage brushless excitation method for hybrid excitation synchronous generator," *IEEE Trans. Magn.*, vol. 51, no. 6, pp. 1–11, Jun. 2015, doi: [10.1109/TMAG.2014.2375325](https://doi.org/10.1109/TMAG.2014.2375325).
- [20] S. Hlioui, L. Vido, Y. Amara, M. Gabsi, A. Miraoui, and M. Lécrivain, "Magnetic equivalent circuit model of a hybrid excitation synchronous machine," *COMPEL Int. J. Comput. Math. Electr. Electron. Eng.*, vol. 27, no. 5, pp. 1000–1015, Sep. 2008, doi: [10.1108/03321640810890735](https://doi.org/10.1108/03321640810890735).
- [21] Y. Xia, H. Jiang, X. Yi, Z. Wen, and Y. Chen, "Parameter optimization of hybrid excitation permanent magnet synchronous motor," in *Proc. 21st Int. Conf. Electr. Mach. Syst. (ICEMS)*, Oct. 2018, pp. 398–401, doi: [10.23919/ICEMS.2018.8549262](https://doi.org/10.23919/ICEMS.2018.8549262).
- [22] Q. Wang and S. Niu, "Design, modeling, and control of a novel hybrid-excited flux-bidirectional-modulated generator-based wind power generation system," *IEEE Trans. Power Electron.*, vol. 33, no. 4, pp. 3086–3096, Apr. 2018, doi: [10.1109/TPEL.2017.2704103](https://doi.org/10.1109/TPEL.2017.2704103).
- [23] L. Zhang, Y. Fan, C. Li, and C. Liu, "Design and analysis of a new six-phase fault-tolerant hybrid-excitation motor for electric vehicles," *IEEE Trans. Magn.*, vol. 51, no. 11, pp. 1–4, Nov. 2015, doi: [10.1109/TMAG.2015.2447276](https://doi.org/10.1109/TMAG.2015.2447276).
- [24] X. Zhao, S. Niu, and T. W. Ching, "Design and analysis of a new brushless electrically excited claw-pole generator for hybrid electric vehicle," *IEEE Trans. Magn.*, vol. 54, no. 11, pp. 1–5, Nov. 2018, doi: [10.1109/TMAG.2018.2823743](https://doi.org/10.1109/TMAG.2018.2823743).
- [25] Y. Burkhardt, K. Schleicher, and M. Klopzig, "A novel hybrid excited synchronous machine for (H)EV applications," in *Proc. Int. Conf. Electr. Mach. (ICEM)*, Sep. 2014, pp. 353–359, doi: [10.1109/ICELMACH.2014.6960205](https://doi.org/10.1109/ICELMACH.2014.6960205).
- [26] C. Wang, Z. Zhang, Y. Liu, and H. Gao, "Mechanical design and analysis of a high-torque modular hybrid excitation synchronous machine for electric vehicle propulsion applications," *IEEE Trans. Veh. Technol.*, vol. 69, no. 9, pp. 9624–9633, Sep. 2020, doi: [10.1109/TVT.2020.3004942](https://doi.org/10.1109/TVT.2020.3004942).
- [27] S. Wang, Y. Xia, S. Huang, A. Qiu, and X. Wang, "Research on new hybrid excitation PM synchronous generators with tooth harmonic excitation," *COMPEL Int. J. Comput. Math. Electr. Electron. Eng.*, vol. 33, no. 5, pp. 1613–1624, Aug. 2014, doi: [10.1108/COMPEL-11-2013-0345](https://doi.org/10.1108/COMPEL-11-2013-0345).
- [28] X. Zhang, Q. Du, J. Xu, Y. Zhao, and S. Ma, "Development and analysis of the magnetic circuit on double-radial permanent magnet and salient-pole electromagnetic hybrid excitation generator for vehicles," *Chin. J. Mech. Eng.*, vol. 32, no. 1, pp. 100–112, Apr. 2019, doi: [10.1186/s10033-019-0334-x](https://doi.org/10.1186/s10033-019-0334-x).
- [29] X. Zhang, Q. Du, S. Ma, W. Hu, and H. Geng, "Magnetic flux analysis and performance test of permanent magnet and claw-pole electromagnetic hybrid excitation generator for electric vehicle range extender," *Int. J. Electr. Hybrid Vehicles*, vol. 9, no. 3, pp. 1–21, 2017, doi: [10.1504/IJEHV.2017.10008512](https://doi.org/10.1504/IJEHV.2017.10008512).
- [30] X. Gu, Z. Zhang, L. Sun, and L. Yu, "Phase displacement characteristics of a parallel hybrid excitation brushless DC generator," *IEEE Trans. Energy Convers.*, vol. 35, no. 2, pp. 875–885, Jun. 2020, doi: [10.1109/TEC.2020.2973194](https://doi.org/10.1109/TEC.2020.2973194).
- [31] Y. Xia, Z. Wen, Z. Zhu, S. Zhong, Y. Chen, and J. Zhang, "Research on a hybrid excitation PM synchronous generator with stator third harmonic winding excitation," *IET Electr. Power Appl.*, vol. 14, no. 3, pp. 418–425, Feb. 2020, doi: [10.1049/iet-epa.2019.0699](https://doi.org/10.1049/iet-epa.2019.0699).
- [32] L. Sun, Z. Zhang, X. Gu, L. Yu, and J. Li, "Analysis of reactive power compensation effect of a new hybrid excitation brushless DC generator," *IEEE Trans. Ind. Electron.*, vol. 67, no. 5, pp. 3562–3572, May 2020, doi: [10.1109/TIE.2019.2916361](https://doi.org/10.1109/TIE.2019.2916361).
- [33] X. Gu, Z. Zhang, L. Sun, and L. Yu, "Magnetic field enhancement characteristic of an axially parallel hybrid excitation DC generator," *IEEE Trans. Magn.*, vol. 57, no. 2, pp. 1–5, Feb. 2021, doi: [10.1109/TMAG.2020.3012148](https://doi.org/10.1109/TMAG.2020.3012148).
- [34] X. Fu, X. Li, D. Xu, and M. Lin, "Iron loss in permanent magnet-inductor hybrid excitation synchronous generator," *IEEE Trans. Magn.*, vol. 50, no. 1, pp. 1–4, Jan. 2014, doi: [10.1109/TMAG.2013.2278016](https://doi.org/10.1109/TMAG.2013.2278016).
- [35] E. N. Kumar, V. N. Deepak, and K. Ragavan, "A compact expression for cogging torque considering both radial and tangential fields for surface-mounted PM motors," *IEEE Trans. Magn.*, vol. 54, no. 9, pp. 1–12, Sep. 2018, doi: [10.1109/TMAG.2018.2845389](https://doi.org/10.1109/TMAG.2018.2845389).
- [36] A. Dalal, P. Kumar, and R. Roy, "Analytical model for permanent magnet motor with non-linear ferromagnetic material property," in *Proc. IECON 42nd Annu. Conf. IEEE Ind. Electron. Soc.*, Oct. 2016, pp. 1604–1609, doi: [10.1109/IECON.2016.7793345](https://doi.org/10.1109/IECON.2016.7793345).
- [37] M. Jafarboland and M. M. Sargazi, "Analytical modelling of the effect of pole offset on the output parameters of BLDC motor," *IET Electr. Power Appl.*, vol. 12, no. 5, pp. 666–676, Apr. 2018, doi: [10.1049/iet-epa.2017.0703](https://doi.org/10.1049/iet-epa.2017.0703).



**HUIHUI GENG** received the B.S. and M.S. degrees from the Shandong University of Technology, Zibo, China, in 2015 and 2018, respectively, where she is currently pursuing the Ph.D. degree. Her research interests include the hybrid excitation generator and starter generator technology.



**XUEYI ZHANG** received the M.S. degree from Guangxi University, in 1990, and the Ph.D. degree from the Shandong University of Science and Technology, in 2011. He primarily works on the research and development of the generator used in vehicle and the electric vehicle technology at the Shandong University of Technology. He has 34 authorized patents, 142 papers, and five monographs. He is a national candidate for China's million talent project and enjoys the special allowance of the State Council. He received the second award of China's national technical invention and six items of the second prizes at provincial and ministerial level.



**LANIAN TONG** received the B.S. degree from the Xi'an University of Technology, Xi An, China, in 1989. He is currently the Director of the Research and Development Center, Shandong Tangjun Ouling Automobile Manufacture Company Ltd. He focuses on key technologies of vehicle electrical technology.



**QINGZHI MA** received the B.S. degree in vehicle engineering from the Shandong University of Technology, in 1992. He currently works as the Technical Director of Shandong Tangjun Ouling Automobile Manufacture Company Ltd. He mainly focuses on the technology of the generator and starter generator for vehicle.



**YUFENG ZHANG** received the B.S. degree from the Shandong University of Science and Technology, in 2016, and the M.S. degree from the Shandong University of Technology, in 2019, where he is currently pursuing the Ph.D. degree. His research interests include the design and manufacture of motor and new energy electric vehicle technology.



**MINGJUN XU** received the B.S. degree in vehicle engineering from the Shandong University of Technology, in 2020, where he is currently pursuing the M.S. degree. His research interests include design and manufacture of generator and motor technology.



**LEI WANG** received the B.S. degree from the Shandong University of Technology, in 2005. He is currently the Director of the Technical Center, Weifang No. 1 Motor Factory Company Ltd. He mainly focuses on vehicle generator technology and driving motor technology for tower crane.

• • •